



(Z)-2-(2-benzylidene-3-oxo-2,3-dihydro[1,4]-benzothiazin-4-yl)acetic acid as a New Corrosion Inhibitor for Mild Steel in hydrochloric acid and Quantum Chemical study

K. Abdu^{1,3}, N. K. Sebbar^{1*}, H. Elmsellem^{2*}, H. Steli⁷, I. Ben Maïmoun³, N. Abad¹, A. Dahdouh⁴, E. M. Essassi^{1,5}, Y. Ouzidan⁶ and M. Ali Shariati⁸

¹Laboratoire de Chimie Organique Hétérocyclique, Centre de Recherche des Sciences des Médicaments, Pôle de Compétences Pharmacochimie, Mohammed V University in Rabat, Faculté des Sciences, Av. Ibn Battouta, BP 1014 Rabat, Morocco.

²Laboratoire de chimie analytique appliquée, matériaux et environnement (LC2AME), Faculté des Sciences, BP. 717, 60000 Oujda, Morocco.

³Laboratoire de Physico-Chimie des Matériaux, Université Abdelmalek Essaâdi, Faculté des Sciences, BP 2121, 93000 tétouan, Morocco.

⁴Laboratoire de Chimie Organique Appliquée Université Abdelmalek Essaâdi, Faculté des Sciences, BP 2121 tétouan, Morocco.

⁵Moroccan Foundation for Advanced Science, Innovation and Research (MASCIR), Rabat Design Center, Rue Mohamed Al Jazouli, Madinat El Irfane, Rabat, Morocco.

⁶Laboratory of Applied Organic Chemistry, Faculty of Science and Technology, University Sidi Mohammed Ben Abdallah, Fez, Morocco

⁷Laboratoire mécanique & énergétique, Faculté des Sciences, Université Mohammed Premier, Oujda, Maroc

⁸Research Department, LLC «Science & Education», and Researcher, All Russian Research Institute of Phytopathology, Moscow Region, Russia.

Received 02 June 2017,
Revised 23 July 2017,
Accepted 26 July 2017

Keywords

- ✓ Benzothiazine;
- ✓ Corrosion;
- ✓ EIS ;
- ✓ Inhibitor;
- ✓ DFT;
- ✓ Fukui function ;
- ✓ MS ;

snounousebbar@gmail.com
h.elmsellem@gmail.com

Abstract

Inhibition performance of [(Z)-2-(2-benzylidene-3-oxo-2,3-dihydro[1,4]-benzothiazin-4-yl)acetic acid]: (P1), has been synthesized and characterized by NMR spectroscopy. The corrosion behavior of MS surface in 1.0 M HCl was investigated by gravimetric, analytical methods potentiodynamic polarization and electrochemical impedance spectroscopy and supported by quantum chemical calculation. The inhibition efficiency of P1 was found to increase with increasing inhibitor concentration. The E% reached 90% at 10⁻³M. Polarization studies showed that this compound was cathodic inhibitor. The inhibition actions of P1 were discussed in view of blocking the electrode surface by means of adsorption of inhibitor molecule obeying Langmuir adsorption isotherm. Data obtained for inhibition efficiency from the two test techniques are in reasonably good agreement with quantum chemical parameters calculated at DFT/B3LYB/6-31G (d, p).

1. Introduction

The study of corrosion inhibition is a very active field of research. Several classes of organic compounds are widely used as corrosion inhibitors for metals in acid environments [1–5]. Experimental means are useful to explain the inhibition mechanism but they are often expensive and time-consuming. Several quantum chemical methods and molecular modeling techniques have been performed to correlate the inhibition efficiency of the inhibitors with their molecular properties [6–10]. Using theoretical parameters helps to characterize the molecular structure of the inhibitors and to propose their interacting mechanism with surfaces [11]. Some studies have shown that the inhibition of the corrosion process is mainly described by the formation of donor–acceptor surface complexes between free or p–electrons of an organic inhibitor, mostly containing nitrogen,

sulfur or oxygen atoms, and a vacant d-orbital of a metal [12–18]. Over the years, 1,4-benzothiazine ring system represents an important class of compounds not only for their theoretical interest but also for their analgesic [19]; anti-viral [20-21] and anti-oxidant [22] activities. In the recent year, research is focused on existing molecules and their modifications in order to reduce their side effects and to explore their other pharmacological and biological effects [23-24]. As a continuation of our research work devoted to the development of N-substituted 1,4-benzothiazine derivatives and evaluating their potential pharmacological activities, the present study aimed to test a new compound named (Z)-2-(2-benzylidene-3-oxo-2,3-dihydro[1,4]-benzothiazin-4-yl)acetic acid (P1) on the corrosion of mild steel in 1 M hydrochloric acid solution. The synthesis of the title compound was performed by hydrolysis reaction with potassium hydroxide of (Z)-methyl-2-(2-benzylidene-3-oxo-2,3-dihydro[1,4]-benzothiazin-4-yl)acetate in ethanol. The resulting reaction mixture was poured into water and acidified with 4 M HCl [25-28]. The molecular structure of (P1) is given in **Figure 1**.

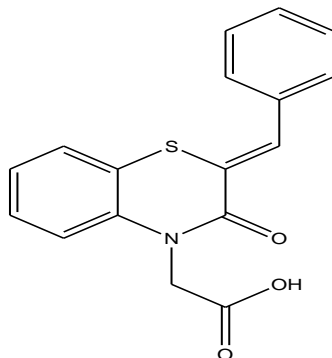
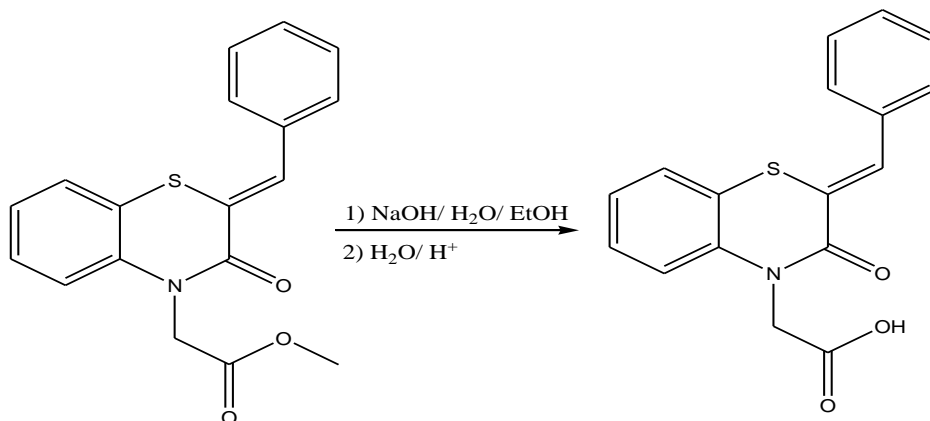


Figure 1. Chemical structure of (Z)-2-(2-benzylidene-3-oxo-2,3-dihydro[1,4]-benzothiazin-4-yl)acetic acid (P1).

2. Experimental

2.1. Synthesis of inhibitor

A solution of potassium hydroxide (12.5 mmol) in water (5 ml) was added to the solution of (Z)-methyl-2-(2-benzylidene-3-oxo-2,3-dihydro[1,4]-benzothiazin-4-yl)acetate (3.07 mmol) in ethanol (20 ml). The resulting reaction mixture was stirred at room temperature for 6 h and the reaction completion was checked by TLC. The reaction mixture was poured into water and acidified with 4 M HCl to form (Z)-2-(2-benzylidene-3-oxo-2,3-dihydro[1,4]-benzothiazin-4-yl)acetic acid as colorless solid. Single crystals suitable for X-ray analysis were obtained by crystallization from dichloromethane under slow evaporation (M.p 84-86 K).



Scheme 1. Synthesis of (Z)-2-(2-benzylidene-3-oxo-2,3-dihydro[1,4]-benzothiazin-4-yl)acetic acid (P1).

The analytical and spectroscopic data are conforming to the structure of the compound formed.

(P1): Yield: 86%; mp: 477K; RMN¹H (DMSO-d₆) δ ppm: 13.42 (s, 1H; OH); 4.73 (s, 2H; NCH₂); 7.65-7.05 (m, 9H, H_{ar}); 7.80(s, 1H, =CH-C₆H₅). **RMN¹³C (DMSO-d₆) δ ppm:** 47.5(NCH₂); 117.7, 126.7, 128.0, 129.1, 129.1, 129.7, 129.7, 130.6, 134.5 (CH_{ar}); 118.1, 120.4, 135.0, 136.7 (Cq); 170.1, 161.5 (C=O).

2.2. Theory and computational details

Quantum chemical calculations are used to correlate experimental data for inhibitors obtained from different techniques (viz., electrochemical and weight loss) and their structural and electronic properties. According to Koopman's theorem [29], E_{HOMO} and E_{LUMO} of the inhibitor molecule are related to the ionization potential (I) and the electron affinity (A), respectively. The ionization potential and the electron affinity are defined as $I = -E_{HOMO}$ and $A = -E_{LUMO}$, respectively. Then absolute electronegativity (χ) and global hardness (η) of the inhibitor molecule are approximated as follows [30]:

$$\chi = \frac{I+A}{2}, \quad \chi = -\frac{1}{2}(E_{HOMO} + E_{LUMO}) \quad (1)$$

$$\eta = \frac{I-A}{2}, \quad \eta = -\frac{1}{2}(E_{HOMO} - E_{LUMO}) \quad (2)$$

Where $I = -E_{HOMO}$ and $A = -E_{LUMO}$ are the ionization potential and electron affinity respectively.

The fraction of transferred electrons ΔN was calculated according to Pearson theory [29]. This parameter evaluates the electronic flow in a reaction of two systems with different electronegativities, in particular case; a metallic surface (Fe) and an inhibitor molecule. ΔN is given as follows:

$$\Delta N = \frac{\chi_{Fe} - \chi_{inh}}{2(\eta_{Fe} + \eta_{inh})} \quad (3)$$

Where χ_{Fe} and χ_{inh} denote the absolute electronegativity of an iron atom (Fe) and the inhibitor molecule, respectively; η_{Fe} and η_{inh} denote the absolute hardness of Fe atom and the inhibitor molecule, respectively. In order to apply the eq.4 in the present study, a theoretical value for the electronegativity of bulk iron was used $\chi_{Fe} = 7$ eV and a global hardness of $\eta_{Fe} = 0$, by assuming that for a metallic bulk $I = A$ because they are softer than the neutral metallic atoms [31]. The electrophilicity has been introduced by Sastri and al. [30], is a descriptor of reactivity that allows a quantitative classification of the global electrophilic nature of a compound within a relative scale. They have proposed the ω as a measure of energy lowering owing to maximal electron flow between donor and acceptor and ω is defined as follows.

$$\omega = \frac{\chi^2}{2\eta} \quad (4)$$

The Softness σ is defined as the inverse of the η [32]

$$\sigma = \frac{1}{\eta} \quad (5)$$

Using left and right derivatives with respect to the number of electrons, electrophilic and nucleophilic Fukui functions for a site k in a molecule can be defined as [32]:

$$f_k^+ = P_k(N+1) - P_k(N) \quad \text{for nucleophilic attack} \quad (6)$$

$$f_k^- = P_k(N) - P_k(N-1) \quad \text{for electrophilic attack} \quad (7)$$

$$f_k^{\cdot} = [P_k(N+1) - P_k(N-1)]/2 \quad \text{for radical attack} \quad (8)$$

3. Results and discussion

3.1. Gravimetric measurements

The corrosion rate of MS specimens after exposure to 1M HCl solution with and without the addition of various concentrations of (Z)-2-(2-benzylidene-3-oxo-2,3-dihydro[1,4]-benzothiazin-4-yl)acetic acid (**P1**) was calculated in $\text{mg cm}^{-2} \text{h}^{-1}$ and the data obtained are given in Table 1.

The inhibition efficiencies ($E_w\%$) were calculated and the data obtained given in the same Table 1. It can be seen from Table 1 that, the addition of P1 to the aggressive solution reduces the corrosion rate of MS. The corrosion rate decreased and inhibition efficiency increased with increasing inhibitor concentration suggests that the inhibitor molecules act by adsorption on the metal surface [33]. The corrosion behavior of MS in 1 M HCl in the absence and presence of P1 was studied at temperature 308K using weight loss technique and data obtained at time (6h) are shown in Table 1. The corrosion rate (v) is calculated using the following equation:

$$v = \frac{w}{S.t} \quad (9)$$

Where: w is the average weight loss, S the total area, and t is the immersion time. With the corrosion rate calculated, the inhibition efficiency (E_w) is determined as follows:

$$E_w \% = \frac{v_0 - v}{v_0} \times 100 \quad (10)$$

Where: v_0 and v are, respectively, the values of corrosion rate with and without inhibitor.

Table 1: Weight loss values of various concentrations of P1 in 1M HCl solution at 308 K.

Inhibitor	Concentration (M)	v (mg.cm ⁻² h ⁻¹)	E_w (%)
1M HCl	--	0.8200	--
P1	10 ⁻⁶	0.2733	67
	10 ⁻⁵	0.2017	75
	10 ⁻⁴	0.1158	86
	10 ⁻³	0.0831	90

3.2. Adsorption isotherm

The adsorption isotherm that describes the adsorptive behavior of organic inhibitors is important in order to know the mechanism of corrosion inhibition. Basic information dealing with interaction between the inhibitor molecules and the metal surface can be provided by adsorption isotherms. Several adsorption isotherms were attempted to fit the degree of surface coverage values (θ) to adsorption isotherms including Frumkin, Temkin, Freundlich and Langmuir isotherms. The θ values for various concentrations of inhibitor in acidic media have been evaluated from the gravimetric measurements (**Table 2**). The best fit was obtained in the case of Langmuir isotherm which assumes that the solid surface contains a fixed number of adsorption sites and each site holds one adsorbed species [33]. The plot of C_{inh}/θ vs. C_{inh} (Figure 2) yields a straight line with correlation coefficient of 0.999 for both mediums providing that the adsorption of P1 on the MS surface obeys Langmuir adsorption isotherm. This isotherm can be represented as [34]:

$$\frac{C}{\theta} = \frac{1}{K} + C \quad (11)$$

Where C_{inh} is the molar concentration of the inhibitor and K_{ads} is the equilibrium constant for the adsorption-desorption process. The value of K_{ads} (**Figure2, Table2**) was found to be $3.91 \times 10^5 M^{-1}$ in 1.0 M HCl.

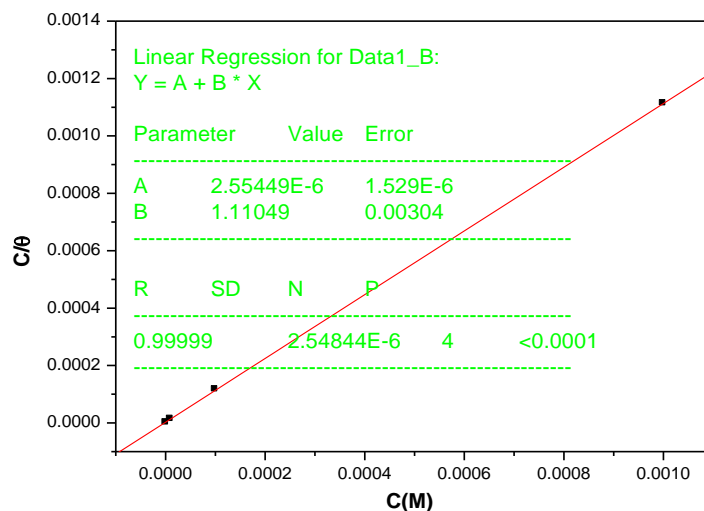


Figure 2: Langmuir isotherm of MS in the 1M HCl in presence P1 calculated by weight loss technique at 308K.

The relatively high value of adsorption equilibrium constant reflects the high adsorption ability of P1 on MS surface [34-35]. The K_{ads} is related to the standard free energy of adsorption, by the following equation (12):

$$\Delta G_{ads} = -RT \cdot \ln(55,5 \cdot K) \quad (12)$$

Where R is gas constant and T is absolute temperature of experiment and the constant value of 55.5 is the concentration of water in solution in mol L⁻¹.

The value was calculated as -43.24 kJ mol⁻¹ in 1.0 M HCl. The negative value of indicates the spontaneity of the adsorption process and the stability of adsorbed layer on the MS surface. It is well known that the values of the order of -20 kJ mol⁻¹ or lower indicate a physisorption; those of order of -40 kJ mol⁻¹ or higher involve charge sharing or transfer from the inhibitor molecules to the metal surface to form a coordinate type of bond (chemisorption) [36]. On the other hand, the adsorption phenomenon of an organic molecule is not considered only as a purely physical or chemical adsorption phenomenon. A wide spectrum of conditions, ranging from the dominance of chemisorption or electrostatic effects, arises from other adsorptions experimental data [36]. The thermodynamic parameters for the adsorption process were obtained from this figure 2 are shown in Table 2.

Table 2: Thermodynamic parameters for the adsorption of P1 in 1.0 M HCl on the carbon steel at 308K

Inhibitor	K _{ads} (L mol ⁻¹)	ΔG _{ads} (kJ mol ⁻¹)	Linear coefficient regression (r)
P1	3.9110 ⁵	-43.24	1.11049

3.3. Electrochemical Measurements

The electrochemical measurements were carried out using Volta lab (Tacussel - Radiometer PGZ 100) potentiostat controlled by Tacussel corrosion analysis software model (Voltmaster 4) at static condition. The corrosion cell used had three electrodes. The reference electrode was a saturated calomel electrode (SCE). A platinum electrode was used as auxiliary electrode of surface area of 1 cm². The working electrode was carbon steel of the surface 1cm². All potentials given in this study were referred to this reference electrode. The working electrode was immersed in the test solution for 30 minutes to establish a steady state open circuit potential (E_{ocp}). After measuring the E_{ocp}, the electrochemical measurements were performed. All electrochemical tests have been performed in aerated solutions at 308 K. The EIS experiments were conducted in the frequency range with high limit of 100 kHz and different low limit 0.1 Hz at open circuit potential, with 10 points per decade, at the rest potential, after 30 min of acid immersion, by applying 10 mV ac voltage peak-to-peak. Nyquist plots were made from these experiments. The best semicircle can be fit through the data points in the Nyquist plot using a non-linear least square fit so as to give the intersections with the x-axis.

3.3.1. Tafel Polarization Study

Figure 3 shows anodic and cathodic polarization plots recorded on MS electrode in 1 M HCl in absence and presence of different concentrations of P1 inhibitor. Electrochemical corrosion parameters, such as corrosion potential E_{corr} (mV/SCE), cathodic β_c Tafel slope (mV/dec), the corrosion current density I_{corr} (μA cm⁻²) and inhibition efficiency E_p (%) are given in Table 3.

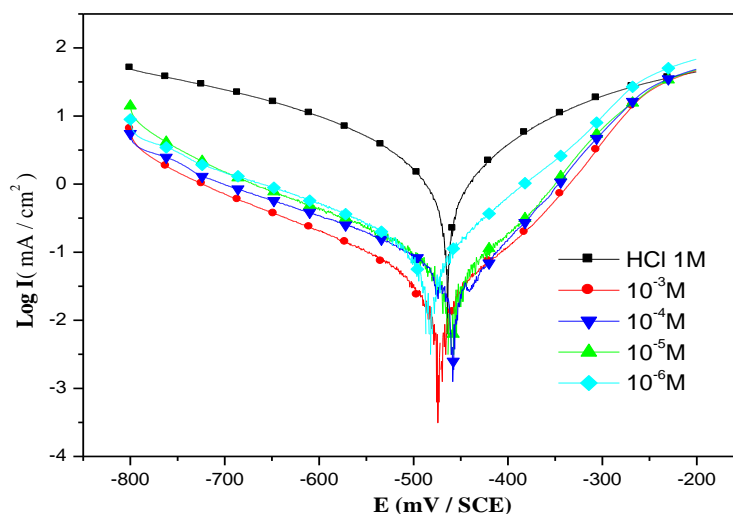


Figure 3: Polarization curves of MS in 1.0 M HCl without and with different concentrations of P1 at 308 K.

From the Figure 3, it can be seen that the addition of P1 causes a remarkable decrease in the corrosion rate i.e., shifts the cathodic curves to lower current densities. In other words, both cathodic and anodic reactions of MS electrode are drastically inhibited after the addition of P1. This may be ascribed to adsorption of inhibitor over the corroded surface of MS[37].

Table 3: Electrochemical parameters and corresponding inhibition efficiency for corrosion of the MS in 1.0 M HCl in the absence and the presence of different concentrations of P1 at 308 K.

	Concentration (M)	$-E_{\text{corr}}$ (mV/SCE)	$-\beta_c$ (mV/dec)	I_{corr} (mA/cm ²)	E (%)
1M HCl	--	465	184	1386	--
P1	10 ⁻⁶	469	123	501	64
	10 ⁻⁵	461	139	358	74
	10 ⁻⁴	460	142	213	85
	10 ⁻³	470	154	137	90

From Table 3, also can find that the corrosion potentials of inhibitor shift slightly in the positive direction in HCl to negative direction. On the other hand, in both mediums, the cathodic Tafel slope β_c change with insignificant trend in anodic and cathodic directions. From previous results, it can be concluded that tested inhibitor probably act as cathodic inhibitor in HCl [38]. As it can be seen from Table 3, in both solutions when the concentration of inhibitor increases the inhibition efficiencies increase, while corrosion current densities decrease. The results obtained in both mediums by potentiodynamic polarization confirm the better inhibitive performance of investigated inhibitor.

3.3.2. Electrochemical impedance spectroscopy (EIS)

In order to better define the effect of our additive and concentration on the corrosion process, Nyquist plots of MS in uninhibited and inhibited acidic solutions containing various concentrations of (Z)-2-(2-benzylidene-3-oxo-2,3-dihydro[1,4]-benzothiazin-4-yl)acetic acid (P1) are shown in Figure 4 in 1.0 M HCl.

The existence of a single semicircle shows a single charge transfer process during dissolution which is unaffected by the presence of inhibitor molecules. Deviations from perfect circular shape are often referred to the frequency dispersion of interfacial impedance, which arises due to surface roughness, impurities, dislocations, grain boundaries, adsorption of inhibitor, and formation of porous layers and in homogenates of the electrode surface [38-39].

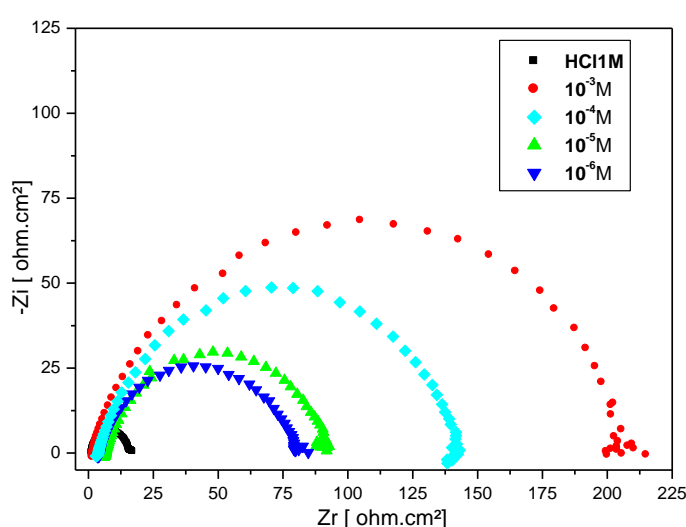


Figure 4: Nyquist plots of MS in 1.0M HCl without and with different concentrations of P1 at 308k.

The diameter of the semicircle increases after the addition of P1 to the aggressive solution. This increase more and more pronounced with increasing inhibitor P1 concentration. The electrochemical parameters derived from *EIS* measurements (including, R_{ct} , transfer charge, double layer capacitance C_{dl} ($\mu\text{F cm}^{-2}$) and the inhibitor efficiency values E (%) are given in Table 4.

Table 4. Characteristic parameters evaluated from *EIS* diagrams with and without P1 at different concentrations.

Inhibitor	Concentration (M)	R_{ct} ($\Omega \text{ cm}^2$)	C_{dl} ($\mu\text{f/cm}^2$)	E_{Rt} (%)
1M HCl	-	15	200	--
P1	10^{-6}	80	123	82
	10^{-5}	90	101	84
	10^{-4}	129	59	89
	10^{-3}	205	45	93

It is evident from the results collected in Table 4, that P1 inhibits the corrosion of MS in 1 M HCl at all the concentrations used, and the inhibition efficiency ($E\%$) increases continuously with increasing concentrations at 308K.

EIS results show also that the R_{ct} values increase and the C_{dl} values decrease with increasing the inhibitor concentration. The increase in R_{ct} value can be attributed to the formation of protective film on the metal/solution interface [39-40]. On the other hand, the decrease in C_{dl} values can result from a decrease in local dielectric constant and/or an increase in the thickness of the electrical double layer. It can be assumed that the decrease of C_{dl} values is caused by the gradual replacement of water molecules by adsorption of inhibitor molecules on the MS surface [41].

EIS spectra of the P1 were analyzed using the equivalent circuit which is shown in Figure 5. Indicates that a single charge transfer reaction and fits well with our experimental results. The constant phase element, CPE, is introduced in the circuit instead of a pure double layer capacitor to give a more accurate fit [42].

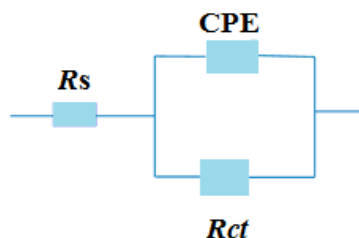


Figure 5: Equivalent circuit model used to fit experimental *EIS*.

3.4. Quantum chemical calculations

The chemical reactivity can be explained according to the frontier molecular orbital theory, by the interaction between the HOMO (the highest occupied molecular orbital) and LUMO (lowest unoccupied molecular orbital) of the reacting species. All the global chemical indexes are summarized in Table 5. The FMOs (HOMO and LUMO) are very important for describing chemical reactivity. The HOMO containing electrons, represents the ability (E_{HOMO}) to donate an electron, whereas, LUMO haven't not electrons, as an electron acceptor represents the ability (E_{LUMO}) to obtain an electron. The energy gap between HOMO and LUMO determines the kinetic stability, chemical reactivity, optical polarizability and chemical hardness–softness of a compound [43]. Firstly, in this study, we calculated the HOMO and LUMO orbital energies by using B3LYP method with 6-31G(d,p). All other calculations were performed using the results with some assumptions. The higher values of E_{HOMO} indicate an increase for the electron donor and this means a better inhibitory activity with increasing adsorption of the inhibitor on a metal surface, where as E_{LUMO} indicates the ability to accept electron of the molecule. The adsorption ability of the inhibitor to the metal surface increases with increasing of E_{HOMO} and decreasing of E_{LUMO} . The HOMO and LUMO orbital energies and image of P1 were performed and were shown in Table 5 and Figure 6. High ionization energy ($I = 6.556 \text{ eV}$, $I = 6.731 \text{ eV}$ in gas and aqueous phases respectively) indicates high stability [44], the number of electrons transferred (ΔN) was also calculated and tabulated in Table 5. The $\Delta N < 3.6$ indicates the tendency of a molecule to donate electrons to the metal surface [45-46].

Table 5. Quantum chemical descriptors of the studied inhibitors at B3LYP/6-31 G** in gaseous (G) and aqueous (A) phases and the inhibition efficiencies as given in [47, 48].

Inhibitor	Phase	TE (eV)	E_{HOMO} (eV)	E_{LUMO} (eV)	Gap ΔE (eV)	μ (D)	IP (eV)	EA (eV)	χ (eV)	η (eV)	ω	σ	ΔN
P1	G	-36305.9	-6.556	-0.100	6.456	1.7235	6.556	0.100	3.328	3.228	1.715	0.309	0.5687
	A	-36306.3	-6.731	-0.113	6.618	2.701	6.731	0.113	3.422	3.309	1.769	0.3022	0.5407

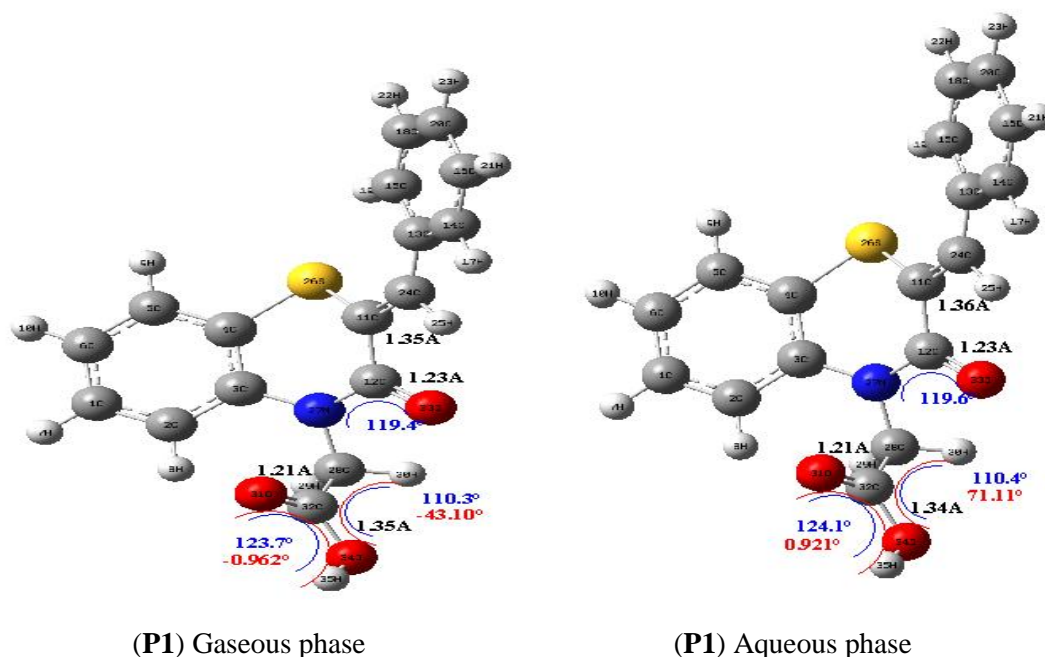


Figure 6: Optimized molecular structures and selected dihedral angles (red), angles (blue) and bond lengths (black) of the studied inhibitors calculated in gaseous and aqueous phases using the DFT at the B3LYP/6-31G level.

To get some insight into the local reactivity of the studied inhibitors, the Fukui functions were computed since they are the relevant reactivity indicators in the electron-transfer controlled reactions such as corrosion inhibition process [49, 50]. Their values are used to identify which atoms in the inhibitors are more prone to undergo an electrophilic or a nucleophilic attack. For a system of N electrons, independent single-point calculations were made for corresponding $N+1$ and $N-1$ electron systems. The resulting natural population analysis yields to $P_k(N-1)$, $P_k(N)$, and $P_k(N+1)$, the population for all atoms k . In a finite-difference approximation from Mulliken population analysis of atoms in molecules, depending on the direction of the electron transfer, then the condensed Fukui functions were computed using the following equations from the Exact Theory [50].

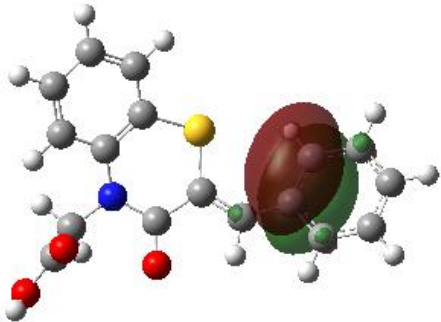
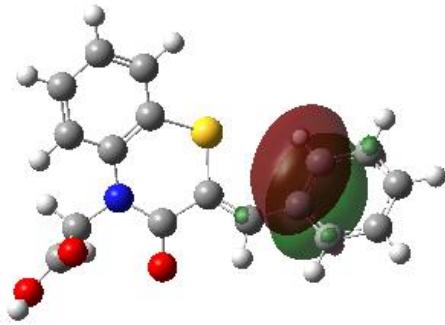
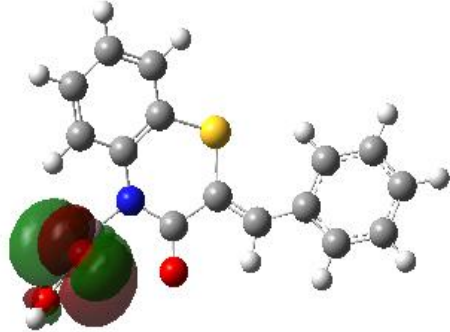
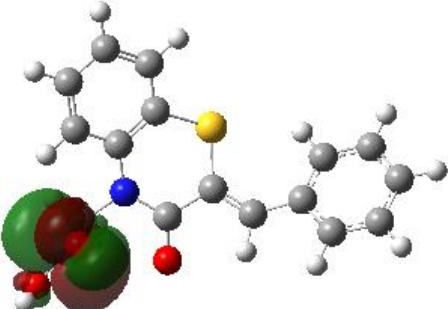
The calculated values of the f_k^+ for all inhibitors are mostly localized on the 1,4-benzothiazine ring. Namely C_4 , C_{11} , C_{24} , S_{26} and O_{33} , indicating that the 1,4-benzothiazine rings will probably be the favorite site for nucleophilic attacks [51-52]. The results also show that S_{26} atom is suitable site to undergo both nucleophilic and electrophilic attacks, probably allowing them to adsorb easily and strongly on the MS surface.

The geometry of P1 in gaseous and aqueous phases (**Figure 6**) was fully optimized using DFT based on Beck's three parameters exchange functional and Lee–Yang–Parr nonlocal correlation functional (B3LYP)[53-54] and the 6-31G. The optimized molecular and selected angles, dihedral angles and bond lengths of P1 are given in (**Figure 6**). The optimized structure shows that the molecule P1 has a non-planar structure. The HOMO and LUMO electrons density distributions of P1 are given in (**Table 7**).

Table 6: Pertinent natural populations and Fukui functions of P1 calculated at B3LYP/6-31G in gaseous (G) and aqueous (A) phases.

Atom <i>k</i>	Phase	$P(N)$	$P(N+1)$	$P(N-1)$	f_k^+	f_k^-	f_k^0
C ₄	G	6,4272	6,20563	6,21194	0,2216	0,2153	0,0032
	A	6,2208	6,22028	6,20727	0,0005	0,0135	0,0065
C ₁₁	G	6,535	6,37698	6,28277	0,1580	0,2522	0,0471
	A	6,29807	6,3897	6,28214	0,0916	0,0159	0,0538
C ₂₄	G	6,19477	6,28642	6,09396	0,0916	0,1008	0,0962
	A	6,17382	6,31624	6,08248	0,1424	0,0913	0,1169
S ₂₆	G	15,12578	15,70345	15,41056	0,5777	-0,2848	0,1464
	A	15,64511	15,72729	15,35615	0,0822	0,2890	0,1856
O ₃₃	G	8,637	8,68801	8,56456	0,0510	0,0724	0,0617
	A	8,63816	8,72246	8,60488	0,0843	0,0333	0,0588

Table 7: The HOMO and the LUMO electrons density distributions of P1 in gaseous and aqueous phases computed at B3LYP/6-31G level for neutral forms.

Inhibitor	Type of MO	Gaseous Phase	Aqueous Phase
P1	HOMO		
	LUMO		

After the analysis of the theoretical results, we can say that the molecule P1 have a non-planar structure. In fact, the CH₂ group is almost perpendicular to the [1,4]-benzothiazine core.

Conclusion

According to experimental and theoretical findings, it could be concluded that:

- (Z)-2-(2-benzylidene-3-oxo-2,3-dihydro[1,4]-benzothiazin-4-yl)acetic acid (P1) is a good corrosion inhibitor for the MS protection in both acid solutions. The inhibitory efficiency of this compound depends on its concentration in both acid solutions.

- EIS plots indicated that R_{ct} values increase and C_{dl} values decrease with increasing inhibitor concentration.
- Polarization curves indicated that P1 act as a cathodic type inhibitor.
- The adsorption of P1 on the MS surface from two acid solutions follows Langmuir adsorption isotherm. The thermodynamic parameters suggest that this inhibitor P1 is strongly adsorbed on the MS surface.
- The quantum chemical parameters are obtained and discussed in view of experimental results

References

1. Shaker M.A., Abdel-Rahman H.H., *Am. J. Appl. Sci.* 4 (2007) 554.
2. Xia S., Qiu M., Yu L., Liu F., Zhao H., *Corros. Sci.* 50 (2007) 2021.
3. El-Naggar M.M., *Corros. Sci.* 49 (2007) 2226.
4. Wang H.L., Liu R.B., Xin J., *Corros. Sci.* 46 (2004) 2455.
5. Larabi L., Harek Y., Benali O., Ghalem S., *Prog Org Coat.* 54 (2005) 256.
6. Gece G., *Corros. Sci.* 50 (2008) 2981.
7. Khalil N., *Electrochim. Acta.* 48(2003)2635.
8. Behpour M., Ghoreishi S.M., Soltani N., Salavati-Niasari M., Hamadani M., Gandomi A., *Corros. Sci.* 50 (2008) 2172.
9. Awad M.K., Issa R.M., Atlam F.M., *Mater. Corros.* 60(2009)813.
10. Awad M.K., *J. Electroanal Chem.* 567(2004)219.
11. Quraishi M.A., Sardar R., Jamal D., *Mater. Chem. Phys.* 71(2001) 309.
12. Issa R.M., Awad M.K., Atlam F.M., *Mat. Corros.* 61(2010) 709.
13. Amina M.A., Mohsenb Q., Hazzazic O.A., *Mater. Chem. Phys.* 114(2009)908.
14. Scendo M., *Corros. Sci.* 49(2007)2985.
15. Sahin M.S., Gece G., Karc F., Bilgic S., *J. Appl. Electrochem.* 38(2008)809.
16. Lashkari M., Arshadi M.R., *Chem. Phys.* 299(2004)131.
17. Jamalizadeh E., Hosseini S.M.A., Jafari A.H., *Corros. Sci.* 51(2009)1428.
18. Gece G., Bilgic S., *Corros. Sci.* 51(2009) 1876.
19. Wammack, R., Remzi, M., Seitz, C., Djavan, B., Marberger, M., *Eur. Urol.* 41(2002)596–601.
20. Malagu K., Boustie J., David M., Sauleau J., Amoros M., Girre R. L., Sauleau A., *Pharm. Pharmacol. Commun.* 4(1998)57–60.
21. Rathore B. S., Kumar M., *Bioorg. Med. Chem.* 14 (2006) 5678–5682.
22. Zia-ur-Rehman M., Choudary J. A., Elsegood M. R. J., Siddiqui H. L., Khan, K. M., *Eur. J. Med. Chem.* 44 (2009) 1311–1316.
23. Sebbar, N. K., Mekhzoum, M. E. M., Essassi, E. M., Zerzouf, A., Talbaoui, A., Bakri, Y., Saadi, M., Ammari, L. E., *Res Chem Intermed.* 42 (2016) 6845–6862.
24. Anupama K.K., Ramya K., Shainy K.M., Joseph A., *Chem. Phys.* 167 (2015) 28–41.
25. Sebbar N. K., Ellouz M., Essassi E. M., Saadi M., El Ammari, L., *IUCr Data.* (2016). 1, x161012.
26. Ellouz M., Sebbar N. K., Ouzidan Y., Essassi E. M., Mague J.T., *IUCr Data* . (2017a). 2, x170097.
27. Ellouz M., Sebbar N. K., Boulhaoua M., Essassi E. M., Mague J.T., *IUCr Data* . (2017b). 2, x170646.
28. Sebbar N. K., Abdelfettah Z., Ellouz M., Essassi E. M., *J. Mar. Chim. Heterocycl.* 14(1) (2015)1-38.
29. Pearson R.G., *Inorg. Chem.* 27 (1988) 734.
30. Sastri V.S., Perumareddi J.R., *Corrosion.* 53 (1997) 617.
31. Elmsellem H., Nacer H., Halaimia F., Aouniti A., Lakehal I., Chetouani A., Al-Deyab S. S., Warad I., Touzani R., Hammouti B., *Int. J. Electrochem. Sci.* 9(2014)5328.
32. Udhayakala P., Rajendiran T. V., Gunasekaran S., *Journal of Chemical, Biological and Physical Sciences* A, 2(3) (2012)1151–1165.
33. Bentiss F., Lagrenee M., Traisnel M., Hornez J. C., *Corros. Sci.*, 41 (1999) 789.
34. Elmsellem H., Youssouf M. H., Aouniti A., Ben Hadd T., Chetouani A., Hammouti B., *Russian, Journal of Applied Chemistry*, 87(6) (2014) 744–753.
35. Fouda A.S., Shalabi S.K., Elewady G.Y., Merayyed H.F., *Int. J. Electrochem. Sci.* 9 (2014) 7038–7058.
36. Elmsellem H., Basbas N., Chetouani A., Aouniti A., Radi S., Messali M., Hammouti B., *Portugaliae Electrochimica Acta* 2 (2014) 77.
37. Lebrini M., Robert F., Lecante A., Roos C., *Corros. Sci.*, 53 (2) (2011) 687.

38. Kedam M., Mattos O.R., Takenouti H., *J. Electrochem. Soc.*, 128 (2) (1981) 257.
39. Chakib I., Elmsellem H., Sebbar N. K., Lahmidi S., Nadeem A., Essassi E. M., Ouzidan Y., Abdel-Rahman I., Bentiss F., Hammouti B., *J. Mater. Environ. Sci.* 7(6) (2016) 1866-1881.
40. Sen K.D., Jorgenson C., *Springer, Berlin.* 66 (1987).
41. Lukovits I., Kalman E., Zucchi F., *Corrosion.* 57 (2001) 3.
42. Khaled K. F., *Applied Surface Science*, 256(22) (2010) 6753.
43. Govindarajan M., Karabacak M., *Spectrochim. Acta Part A Mol. Biomol. Spectrosc.* 85 (2012) 251.
44. Bendaha H., Elmsellem H., Aouniti A., Mimouni M., Chetouani A., Hammouti B., *Physicochemical Mechanics of Materials.* 1 (2016) 111-118.
45. Lukovits I., Kalman E., Zucchi F., *Corrosion.* 57 (2001) 3.
46. Elyoussfi A., Dafali A., Elmsellem H., Steli H., Bouzian Y., Cherrak K., El Ouadi Y., Zarrouk A., Hammouti B., *J. Mater. Environ. Sci.* 7 (9) (2016) 3344.
47. Verma Chandrabhan, Quraishi M.A., Ebenso E.E., Obot I.B., El Assyry A., *J. Mol. Liq.*, 219 (2016) 647.
48. Sikine M., Elmsellem H., KandriRodi Y., Steli H., Aouniti A., Hammouti B., Ouzidan Y., OuazzaniChahdi F., Bourass M., Essassi E.M., *J. Mater. Environ. Sci.* 7 (12) (2016) 4620-4632.
49. Becke A.D., *Phys. Rev. A.* 38 (1988) 3098.
50. Quijano M.A., Pardav M.P., Cuán A., Romo M.R., Silva G.N., Bustamante R.Á., López A.R., Hernández H.H., *Int. J. Electrochem. Sci.*, 6 (2011) 3729.
51. Kumar S., Ladha D. G., Jha P. C., and Shah N. K., *International Journal of Corrosion* Volume (2013), ID 819643, 10 <http://dx.doi.org/10.1155/2013/819643>.
52. Khaled K. F., *Applied Surface Science*, 256(22) (2010) 6753.
53. Verma C., Quraishi M.A., Gupta N. K., *Ain Shams Eng. J.* <http://dx.doi.org/10.1016/j.asej.2016.07.003>.
54. Lee C., Yang W., Parr R.G., *Phys. Rev. B.* 37 (1988) 785.

(2017) ; <http://www.jmaterenvirosci.com/>